Spot-o-matic: A Test Bed for Measuring Intrapixel Variation in Near Infrared Focal Plane Arrays

Michael Borysow

Adviser: Wolfgang Lorenzon

A Thesis presented for the degree of
Bachelor of Science

SNAP Group
Department of Physics
University of Michigan
USA

April 2004

Dedicated to

My father, whom despite all the trouble I've caused, and tuition bills I've left him, has always been there to support me in whatever crazy things I decided to pursue.

Spot-o-matic: A Test Bed for Measuring Intrapixel Variation in Near Infrared Focal Plane Arrays

Michael Borysow

Submitted for the degree of Bachelor of Science
April 2004

Abstract

The Michigan SNAP group is heading the characterization of the HgCdTe detectors which will be responsible for NIR photon detection in the SNAP focal plane. In order to characterize these devices, a testing facility had to be designed and constructed. We have designed and built such a facility, and developed and/or acquired the necessary software and hardware in order to measure various performance aspects of the detectors. I attempt here to show proof of concept for our facilities using first the CCD from a consumer level webcam. This thesis will focus on our spot projection system, fondly referred to as the "spot-o-matic," and the intrapixel variation measurements resulting from its use.

Declaration

The work in this thesis is based on research carried out by the Michigan SNAP Group, the Department of Physics, the University of Michigan, USA. No part of this thesis has been submitted elsewhere for any other degree or qualification and it is all my own work unless referenced to the contrary in the text.

Acknowledgements

Without the wisdom and advice of many of my colleagues, this work would have been exceedingly more difficult if not impossible.

I would especially like to thank my adviser, Wolfgang Lorenzon for all he's done for me. He's been a terrific help in my academic carreer. He has looked out for me and insured that I haven't made a fool of myself in front of my peers and he's also always made me feel like an appreciated and valuable contributor to whatever projects we've worked on together.

I would also like to thank the following people for their intellectual banter and other forms of help:

Greg Tarlé
Michael Schubnell
Andrew Tomasch
Matt Brown
Tim Chambers

And of course, Nate Barron, who actually constructed the spot-o-matic, without which I wouldn't have been able to do most of the analysis in this thesis.

Contents

List of Figures

List of Tables

Chapter 1

Introduction

Recent observations of our universe have left us with the surprising conclusion that the rate of expansion of the universe is accelerating. [1] In a matter dominated universe, with gravity as the primary force for any acceleration, this is a surprising result indeed. In this scenario the expansion of the universe should in fact be decelerating. However, this is not the case. Something must be driving this acceleration, and the culprit to which the blame has been attributed, is something that in truth we know nearly nothing about. That culprit is called dark energy.

To learn more about the means ("dark energy") by which the acceleration is taking place, it would help to have a better knowledge of the expansion history. The proportion of dark energy to ordinary matter over the history of the universe will be helpful in our understanding. We need to discern the acceleration of the universe as a function of its age.

In order to make these measurements, we need a way to sample the acceleration of the universe at many different epochs. Luckily, there is a clever method available for this. Observing the redshift and apparent magnitude of some form of stellar standard candle provides us with a measurement of both the distance and the velocity of the object. We have such a standard candle: The type IA supernova.

The use of type IA supernovae for these measurements is quite common, [2, 3] but in general, these observations are limited to the visible spectrum. As we observe stellars objects that are farther and farther away, we discover that their spectrum is shifted to longer wavelengths. This behavior is called redshift and is quantified by a value z. Supernovae with $z > 0.9$ are shifted from their rest-frame visible emission at $\sim$500nm into the near infrared (NIR). The silicon CCDs commonly used for astronomical purposes have an upper cut-off of about 1000 nanometers, limiting their usefulness for analyzing higher redshift supernovae. High redshift supernovae are extremely useful in constraining the systematic uncertainty in several of the parameters we are interested in. [4] In order to make use of these supernovae, some detector sensitive to photons having wavelength of $\lambda > 1000nm$ is required. [5, 6]

The Michigan SNAP group is leading the characterization of the NIR sensitive focal plane arrays (FPAs) for the Supernova Acceleration Probe (SNAP) telescope. In order to achieve the best performance from these devices we need to perform a complete and accurate optical and electrical characterization for each device. In order to meet science requirements we must measure the following:

- FPA Sensitivity
  - Readout Noise
  - Dark Current
  - Relative and Absolute Quantum Efficiency
- FPA Uniformity
  - Inter-pixel Variations
  - Intra-pixel Variations
  - Gain
  - Linearity
- FPA stability
  - Latent Charge
  - Thermal Stability

The importance of intra-pixel variation measurements is not immediately obvious. Most modern astronomical telescopes oversample the sky. That is, the characteristic size of objects falling on the detector is larger than a pixel. Thus, oversampling limits the size of any kind of survey of the sky. The SNAP telescope intends to take measurements of thousands of supernovae over its lifetime, and this requires a much wider survey than most telescopes are able to perform. SNAP will be undersampling the sky.

Undersampling makes it necessary to understand intra-pixel variation very well. If the characteristic size of objects falling on the detector is smaller than a pixel, we must be confident, that wherever within the pixel the object falls, the same apparent magnitude can be extracted. There are various methods for recovering any lost information from undersampling, including dithering and drizzling. [7]

The focus of this thesis will be the Michigan SNAP group's unique ability to measure intra-pixel variations to high precision. We are able to do this through the use of a device built at Michigan known fondly as the "spot-o-matic."

1.1 Spot-o-matic

The spot-o-matic is a spot projection system developed at Michigan as an adaptation for use in the NIR of a similar system used at Lawrence Berkeley Laboratory. [8]

Our full spot-o-matic system consists of a pinhole projector mounted on a three-dimensional motorized translation stage purchased from National Aperture, Inc. The stage and pinhole projector can be seen in Figure 1.1. Also included in the system is all the software written in Labview and C by myself for its automated operation. The stage has three independent linear axes, each having a 78 mm travel range and mounted atop each other. The model number for each axis is the MM-4M-EX-80. The stage is driven by the MC-4SA Servo Amplifier System, also from National Aperture. The actual control is done through interfacing with the NI-7344 PCI Card from National Instruments.

Figure 1.1: A side-on view of the spot projection system (spot-o-matic) as set up for testing with a webcam CCD. The light is carried into the spot-o-matic from a fiber optic bundle on the left.

Due to concerns with light output stability over time, we have purchased a new light source from Oriel that will satisfy our stability requirements. It is a 50 Watt Quartz-Tungsten-Halogen lamp based system in an Oriel PhotoMax lamp housing. The output intensity is regulated by a 49931 DC regulated radiometric power supply tied into a feedback loop with a light intensity controller which samples the light intensity near the work plane. Light will be carried using a liquid light guide from the lamp housing to the end of the spot projector. The light will pass through a small pinhole which will be demagnified 10 times and be imaged about 3.2 cm past the other end of the spot-o-matic, as shown in Figure 1.2.

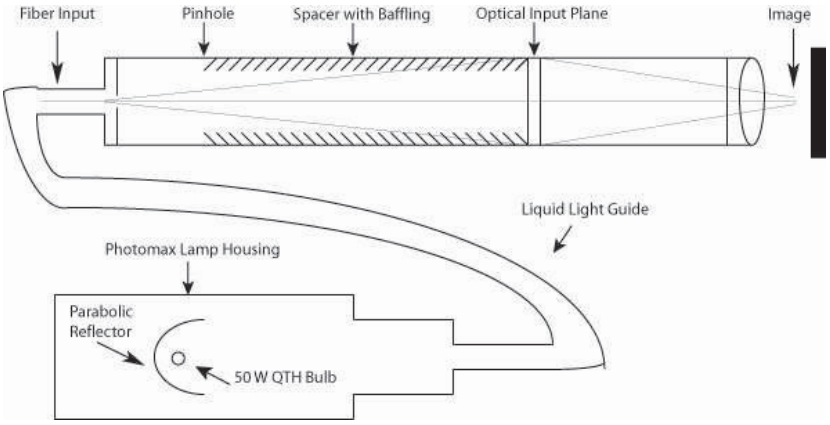

Figure 1.2: A diagram showing the current setup of the spot projection system (spot-o-matic) as used for testing with a webcam CCD (see Chapter 5). The light is produced by a 50 Watt Quartz-Tungsten-Halogen bulb, collected by a parabolic reflector, sent through a liquid light guide, passed through a 10 micron pinhole, and focused to a small spot on the CCD.

Chapter 2

Characterizing the XYZ Stage

The motorized translation stage we are using was purchased from National Aperture, Inc. and is composed of three model MM-4M-EX-140 stages each with a 78 mm travel range, mounted atop each other to form an orthogonal frame of reference in x, y, and z. The stage comes with the appropriate specifications to make measurements accurate to the micron. While this is phenomenal for some uses, we intend to take many measurements over an 18 micron by 18 micron area. Why remain accurate within 5 to 10 percent, when characterizing and examining the properties of our stage can lead to accuracies at the single percent level.

Several measurements were taken in order to understand more precisely the motion of the stage. For example, we may measure that the reported position of the stage drifts consistently by a certain amount as it moves in one direction. This knowledge can be used to compensate for that behavior in software. These types of characterizations allow us to more accurately ascertain the true position of the stage as well as any associated error in position.

2.1 Backlash

In any mechanical system, backlash is inevitable. Backlash is often referred to as "slop" or "slack" in the system. In a translation stage, backlash exhibits itself by having the stage "lose" its position slightly when changing direction.

2.1.1 Explanation of Backlash Effects

Suppose the carriage on our stage is moving along in the positive direction, and we decide to change the direction of motion. The lead-screw begins turning in the opposite direction, but the carriage does not actually move immediately. It requires a little extra turning to make up for the "slop" in the interface between the carriage and the screw. The problem arises when we try to read the position of the carriage from the encoders. The encoders are incorporated in such a way that they measure the amount by which the lead-screw has been turned. So, in the example just given, even though the carriage does not move immediately after the direction change, when the software queries the encoders, they will report that it in fact has been moving.

Backlash is fairly easy to compensate for in software. All that one needs to do is keep as a reference the direction of the last movement. If the current move is going in the opposite direction, we reset the encoder to a value that will make the stage travel further than it normally would by the known backlash amount.

Here is a quick example of compensating for backlash in our current system. Let us assume that we have just made a movement in the negative direction that has landed us in a position that the encoder reads as 0 microns. We now wish to move to the location defined by the encoder as +5 microns. We know that we are changing directions, so we need to account for backlash. Let us assume that the backlash is known to be 1 micron in this axis. We reset the encoder so that it thinks it is actually at the location -1 micron. We now begin the motion. The first micron of travel is compensation for the backlash in the screw. The following 5 microns are the actual move that was desired. So, we end up at the position +5 microns, just as requested, and the encoder agrees.

The unfortunate reality of the situation is that the stage arrived with the backlash in each axis measured only to the nearest micron. Using a little ingenuity and our dismantled webcam we knew we could measure it to better precision.

2.1.2 Characterizing the Backlash

It was first necessary to determine a reliable way to measure the backlash of each axis. This turns out to be a trivial procedure for the two axes that move in the plane of the detector, but a slightly more difficult and tedious procedure for the focusing axis. We will begin with the easier axes.

Armed with the knowledge that our spot is roughly gaussian, a simple routine was constructed in order to measure the backlash. A single pixel is read out continuously as the spot is moved back and forth across it in single count (.074 micron) increments and over a range of roughly 30 microns.

Looking at the complete scan in Figure 2.1, it is easy to see that there is a fair amount of structure in the response that, frankly, is not of interest. What we are looking for is a response pattern that meets two criteria. It must remain a common observable shape in consecutive scans, and ideally it should fit well to some known and fairly simple function. As is expected from our knowledge of the spot distribution and the method we are using, there is a shape resembling a gaussian peak in the middle of the scan. This will be used as a reference in locating the physical coordinate of the pixel in each scan.

Limiting our fits to only the range where the pixel response is roughly gaussian, we continue with our analysis. Immediately, we can observe that consecutive scans, as in Figure 2.2 have a measurable offset. Consecutive scans (differing directions) are fit to a gaussian function and the difference between the location of two peaks is recorded as a single measurement of the backlash.

In order to acquire appropriate statistical precision, this back and forth scan is made about 80 times. The distribution of recorded backlashes in each direction for axes 1 and 2 are plotted as histograms in Figure 2.3. The importance of measuring the backlash becomes immediately apparent. First off, for the x axis (axis 1), National Aperture's quoted backlash is 2 microns. We have made a considerably more precise measurement of the backlash which will allow us to know our position along axis 1 more accurately. An even more important

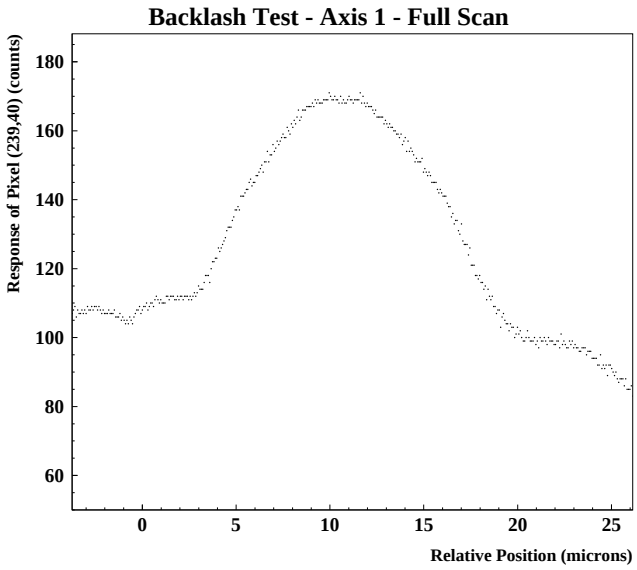

Figure 2.1: The intensity reported by a single pixel as a function of stage position. It is an example of a typical backlash scan. A single pixel is read out at single count (.0749 micron) increments as the spot is moved across it.

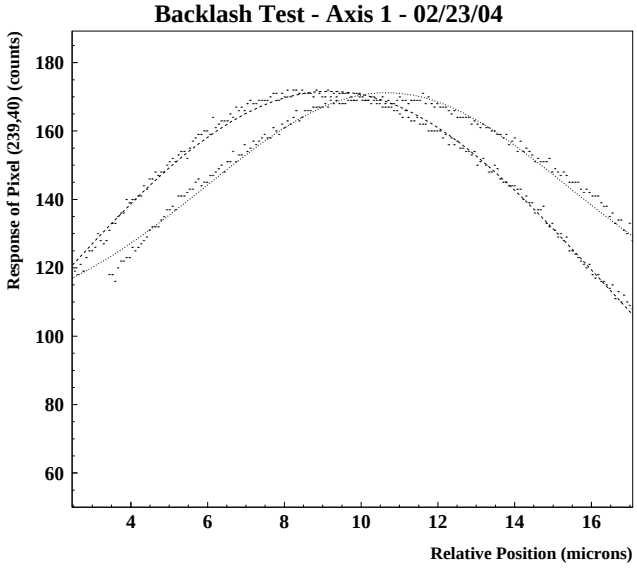

Figure 2.2: An example of two consecutive backlash scans. After the first measurement, shown in Figure 2.1, the stage reverses direction and repeats the same procedure. The range is limited to where the response shows a well behaved peak, and a gaussian is fit to each measurement. The difference in the position of the peaks from consecutive gaussian fits is recorded as a single measurement of the backlash.

observation is the noticeable asymmetry in the backlash[1].

While a difference in the means of the distributions of .07 microns may seem trivial, this is almost precisely one count (the discrete step size of the stage is equal to .0749 microns) and can be easily corrected for. To show the importance of this asymmetry, imagine the following experiment. Imagine an XY grid scan of a single pixel. A full scan like this will likely take at least 20x20 images. As the scan commences, a change in direction will occur 20 times. With an asymmetry of 1 count, over the course of the experiment, we will have drifted in position by 20 counts. This is a drift of 1.5 microns. When observing a pixel that is 18 micron square in dimension, we have shifted in position on the pixel by as much as 8% of a pixel!

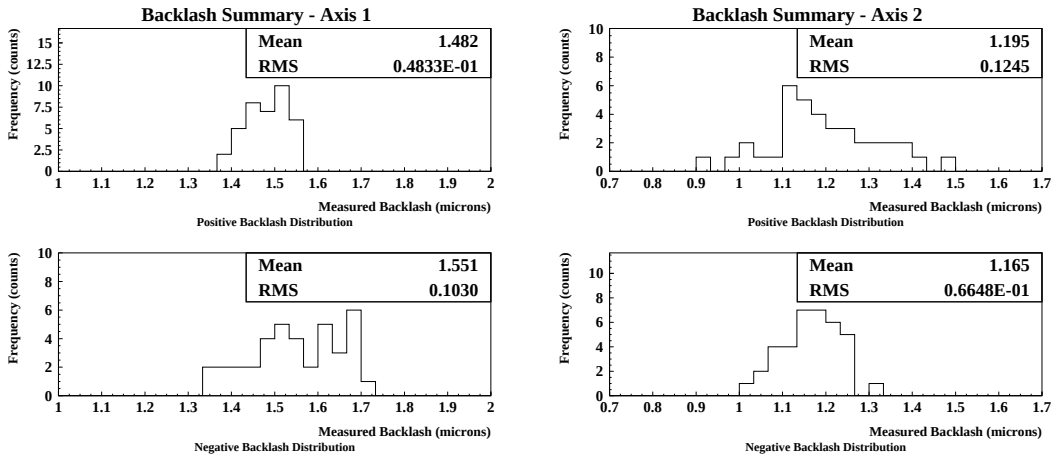

Figure 2.3: Distribution of measured backlashes in each direction for the x axis (left panels), and the y axis (right panels). Positive backlashes are presented in the top distribution. Negative backlashes are plotted in the bottom distribution.

Finally, the focusing axis had to be characterized. Changing direction in this axis will not occur very often, and when it is done, it's usually for the purpose of finding a position and not moving from it, so this axis was less of a worry.

As seen in Section 3.1.1 beginning on page 11, we are able to measure the spot size as a function of distance from focus by scanning the spot over a knife edge at differing z values. As the geometry suggests, we find a more or less linear relation with some curvature very near the focal point. Just as we did with the other two axes, we find a repeatable pattern (in this case, spot size as a function of position) and fit it repeatedly while taking the measurement in differing directions. For more information on the knife edge scans, see Section 3.1.1. The same procedure was used as in that section, only differing in that we scanned in one direction along the axis, and then turned around and repeated the measurement while moving in the opposite direction in Z. Each scan was fit to the absolute value function and a distribution of the difference in consecutive focus positions is plotted in Figure 2.4.

[1]Positive and Negative backlash are defined as follows: Positive backlash refers to the backlash experienced when changing directions *following* a move where the motors changes from a clockwise rotation to a counterclockwise as seen facing down the shaft. The opposite is true for negative backlash.

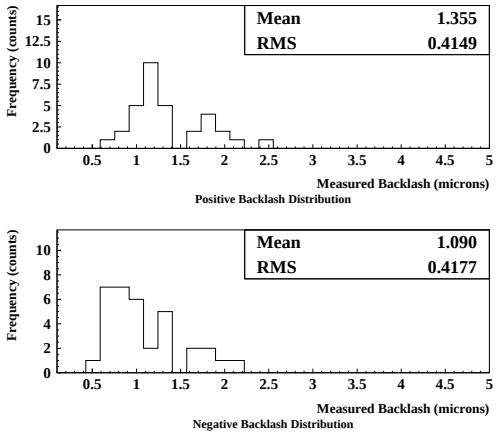

Figure 2.4: Distribution of measured backlashes in each direction for axis 3. Positive backlashes are presented in the top distribution. Negative backlashes are plotted in the bottom distribution.

Immediately one sees a more disturbing trend than was observed with the other two axes. The distribution is considerably more wide, and the difference between the positive and negative backlash is quite extreme. The average asymmetry is 0.3 microns. If this went unaccounted for, the drift after several changes in direction would be very troublesome. It is most worrying in that our setup for real devices will have the end of the spot-o-matic nearly flush with a window. This is necessary due to the extremely short working distance of the spot-o-matic. With this kind of drift it is entirely possible that the spot-o-matic could physically run into the window and become damaged.

It is difficult to make a direct comparison due to the differing natures of the tests used in each case and several hypotheses are currently being debated. The third axis has the largest "burden" to bear. It is carrying the most weight and as of current is not well balanced. As the spot-o-matic is currently set up in a relatively confined mounting space, it was necessary to extend axis 1 (the x axis) almost all the way to one end of its travel range. This results in a certain amount of torque being exerted on axis 3, which may exhibit itself as a larger amount of drift and/or backlash asymmetry.

2.1.3 Accommodating for Backlash

An asymmetric backlash accommodation routine was programmed that is consulted before any stage motion occurs. First, a check is made to see if the direction is changing. If this check returns positive, the appropriate backlash statistic (see Table 2.1) is taken, and the absolute position of the stage is "reset" to a position that is farther away from the destination by the correct amount of counts so as to traverse over the backlash in addition to the desired amount of travel.

Axis	*Backlash (microns)*	
	Positive	*Negative*
X	1.482	1.551
Y	1.198	1.165
Z	1.355	1.090

Table 2.1: Per-axis backlash values for our XYZ translation stage as measured using the method described above.

2.2 Drift

National Aperture has provided us with measured values per-axis for the accuracy of the stage, as given by accuracy for every 25 mm of travel. We would like to verify these values but do not have the necessary equipment to measure this independent of backlash.

Quoted drift from National Aperture, Inc. is shown in Table 2.2.

Axis	*Drift per 25 mm of travel (microns)*
One	0.3
Two	0.3
Three	0.2

Table 2.2: Amount of drift in position per 25 mm of travel for each axis of our XYZ translation stage as reported by National Aperture.

2.3 Repeatability

National Aperture has provided us with a measured values per-axis for the repeatability of the stage. We wish to verify these values for ourselves but have not yet been able.

Quoted repeatability from National Aperture, Inc. is shown in Table 2.3.

Axis	*Repeatability (microns)*
One	0.2
Two	0.3
Three	0.2

Table 2.3: Repeatability of position for each axis of our XYZ translation stage as reported by National Aperture.

Chapter 3

Characterizing the Optics

3.1 Spot Profile

In an ideal testing environment for measuring intra-pixel variations, one would hope to have a spot with infinitesimal width. Due in part to diffraction and Louisville's Theorem, we can only achieve a spot of finite width. With the optical components we purchased, we expected to demagnify by 10 times pinholes of size ranging from 10 microns to 1000 microns, resulting in projected spots of size ranging from 1 to 100 microns. In the case of larger pinholes where diffraction is not the dominating factor in the spot size, we expected a roughly gaussian spot with diameter about 10 times smaller than the pinhole diameter. The light output from a 10 micron diameter pinhole with a 650 nm filter attached can be seen in Figure 3.1.

Figure 3.1: Picture of a piece of the spot-o-matic tube. In the center of the tube is a faint, small red dot. This red dot is light emerging from the 10 micron pinhole after having passed through the fiber optic and through a 650 nm narrow bandpass filter. This red dot is what is imaged by the lens system of the spot-o-matic and onto the FPA.

Due to the nature of our finite sized spot, it will be slightly more difficult to map out the variations within a single pixel. For example, if we had a spot having a uniform power distribution with diameter 5 microns, and we scanned it across a square pixel with dimensions

18 micron by 18 micron, we would acquire a response map which is the convolution of the pixel response function and the relative spot intensity function.

3.1.1 Knife Edge

The most common way of measuring the profile of a beam of particles or, in our case, photons, is to progressively streak the beam across some form of obstruction, often referred to as a knife edge.

Our initial test was comprised of streaking our spot across a razor blade that had been taped in front of the CCD on our webcam, as seen in Figure 3.2. Prior to use, the razor was examined under a microscope to ensure that its edge was straight enough for the measurements we were going to make. We observed the razor to be smooth to the sub-micron level and determined that this was in fact straight and smooth enough for our purposes.

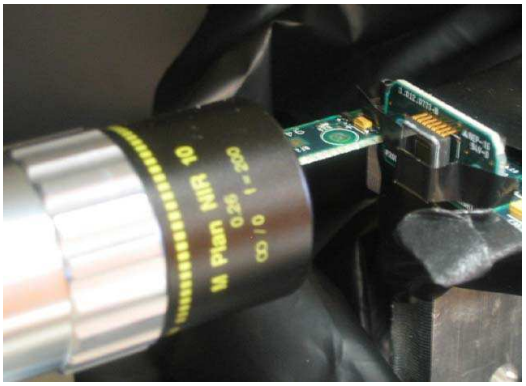

Figure 3.2: Picture of the webcam CCD with the razor blade used for knife edge tests affixed to its bottom. The end of the spot-o-matic can be seen to the left.

Geometry again was a limiting factor. A plastic window is located roughly 2 mm above the CCD itself. This was as close to the CCD as we could place the razor. It is worth noting here, that these tests can and will be repeated using the pixel boundaries on later devices that we will be testing. The pixel boundaries on the HyViSi device, as well as the HgCdTe devices, are very well defined. This will provide a very good method for focusing on these devices.

The test procedure is as follows. The stage is coerced to a location where we know the spot is roughly centered and focused upon the edge of the razor. At this point, what we observe when looking at an image from the CCD, is half of a very large spot with an area covering tens of thousands of pixels. The spot is moved out of focus in the direction of the CCD, and above the razor so that none of the beam is obstructed. The spot is then slowly moved across the razor in single step increments. After each step, the readout from every pixel over the entire CCD is summed and recorded. The result from a single such scan can be seen in Figure 3.3.

This data fits fairly well to the error function, which is represented by

$$erf(z) \equiv \frac{2}{\sqrt{\pi}} \int_0^z e^{-t^2} dt. \tag{3.1}$$

Assuming that our spot profile can in fact be reasonably estimated as gaussian, then this is what we expect. In reality, the image being projected is represented by a two dimensional Airy function. Luckily, a first order approximation of a gaussian is quite reasonable. From this information we can extract a beam size in sigma by fitting to

$$A_0 * erf(\frac{A_1 - A_2}{\sqrt{2} * A_3}) + A_4, \tag{3.2}$$

where A_3 is sigma for the corresponding gaussian profile.

Figure 3.3 shows the smallest ever recorded spot as of April 2004. Using a 10 micron pinhole located 175 mm from the first lens, a spot with sigma of .56 microns was achieved. The data points in the lower plot of Figure 3.3 represent the discretely calculated derivative of the knife edge scan in the plane above it. The severe fluctuation on the right is purely statistical. The bottom plot is *actually* a calculated derivative of the reflection of the above plot, and what appears to be a distribution of data points close to 0 in the top plot is in fact a distribution around nearly 50 and fluctuating slightly.

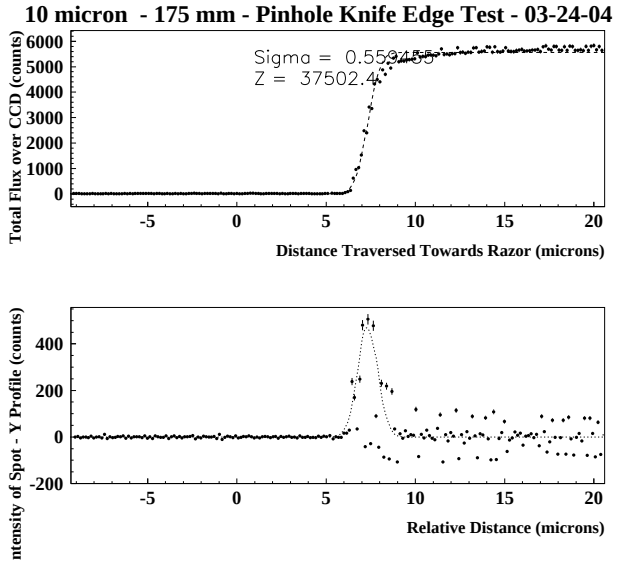

Figure 3.3: Knife edge plot of the smallest spot recorded, with a sigma of .56 microns. The spot is moved (in the plane of the razor) toward the blade, and as the razor begins to obstruct some of the light, the total observed flux decreases. The top plot shows the the integrated flux over the entire CCD recorded as a function of stage position. This data is fit to the error function and sigma is extracted. The approximated profile (bottom) is overlaid with the fit from the data above. The scatter in the bottom plot is purely statistical. The plot is flipped, and the scatter in the bottom plot is actually where the signal is nearly 0 in the top plot, so any small fluctuations taken as a discrete derivative will look large.

Realizations

During the course of these knife edge experiments, several unexpected results arose that initially baffled us, but have slowly come to make sense. Initial knife-edge tests resulted in a 1000 micron pinhole producing a sigma width at focus of 3.5 microns. Taking the spot size to be the FWHM of the distribution, this gives us an estimated spot size of 9.5 microns in diameter. This result implies a demagnification of $\sim$ 100 times, which is an order of magnitude greater than the 10x demagnification expected.

The initial suspect was that perhaps the pinhole was not at the focus of the optics of the spot-o-matic. The quoted focus from the companies that manufactured the lenses is 175 mm. We measured the distance from the first lens to pinhole and found it to be about 164 mm. Thought experiments initially seemed to imply that this would indeed increase the demagnification in the observed direction. However, measuring the minimum spot size at various pinhole distances as shown in Figure 3.4, shows clearly that the the pinhole distance has no measurable effect over a range of 20 mm.

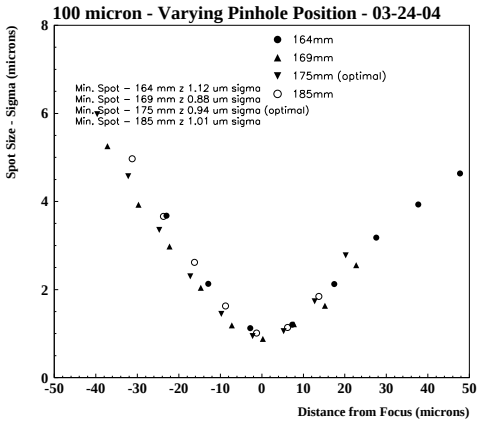

Figure 3.4: From every knife edge, as shown in Figure 3.3, a value sigma representing the size of the spot is extracted. The culmination of many such knife edges at different positions in the focusing axis is shown. Several such scan collections are shown with varying distances between the focusing optics and the pinhole.

After performing a similar analysis for spot size as a function of pinhole size, we find the surprising result (shown in Figure 3.5 (right panel)) that there is nearly no variation in spot size between pinhole sizes of 10 microns and 100 microns. There is however, an observable difference between the 100 micron and 1000 micron pinholes, which can be seen in Figure 3.5 (left panel).

It is worth noting, and this unfortunately wasn't obvious to us as an issue initially, that when viewing the spot out of focus on the CCD in these tests, the defocused spot would appear to have an almost uniform intensity distribution. This can be seen in Figure 3.6. While it was a nice, flat, easy to work with distribution, it really should not have been what was observed. With a little thought, we realized what the problem was.

When looking at Figure 3.7 we can see that there is some space between the output of the fiber and the pinhole. This separation leads to the optical system not actually imaging

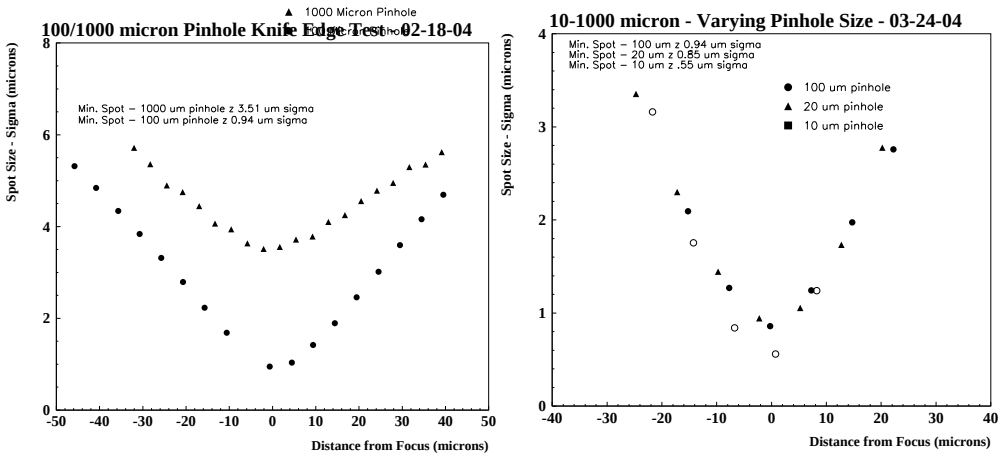

Figure 3.5: Measured spot size as a function of distance from focus for various pinhole sizes. The left figure shows the 1000 micron and 100 micron pinholes. The right figure shows the 10, 20, and 100 micron pinholes.

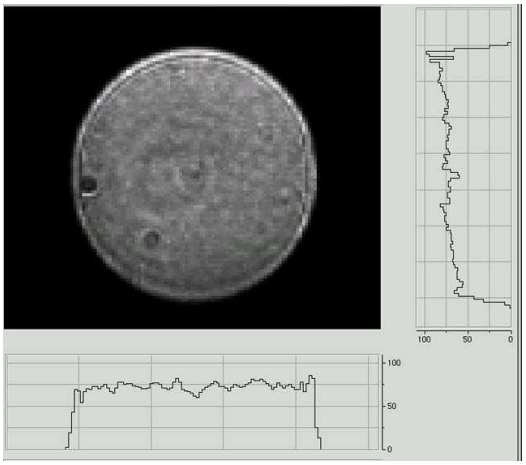

Figure 3.6: Image from the CCD of the spot when far out of focus and when the pinhole is far from the fiber output. Note: Focusing in and out keeps the distribution roughly flat over the entire range of in focus to far out of focus. This image was made using a 100 micron pinhole.

the pinhole. If you look closely at the angles in the image, you will notice that we are underfilling the lens. The real setup is actually more exaggerated of a problem than what is seen in the figure, and we are in fact underfilling the lens to such a degree, that we are practically sending in a beam of parallel light. The 10 times demagnification quoted for the lens is for a point source located at the focus of the system, and thus assumes that the lens is filled. This also very nicely explains why there was no difference in spot size as a function of the distance of the pinhole from the first lens. As we move the pinhole, we are still passing primarily parallel light through the system. The lens "sees" nearly the same thing regardless of where the pinhole is located.

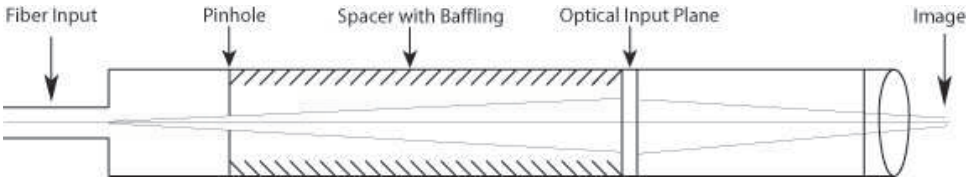

Figure 3.7: An illustration of our problematic setup. Notice that the distanced pinhole forces a severe limitation in the acceptance angle of light passing through, and hence underfills the lens.

Our next step was to place the pinhole as close to the fiber as possible. Immediately we noticed a drastic difference in the images coming out of the CCD of the defocused spot. Where once was observed a circular, flat distribution, now appeared a very bright central point with what seemed to be a radial gradient. This can be seen in Figure 3.8. Compare this to the flat distribution seen in Figure 3.6. Initially this confused us, particularly because the bright spot disappeared on only one side of the focus. That is to say, when focused in front of the CCD, the bright peak would appear, but when focused beyond the CCD, it would vanish. We eventually found the culprit to be a reflection from inside the tube of the spot-o-matic. After improving our baffling, the bright spot vanished.

In the spot-o-matic's final configuration, we simulate the pinhole being flush with the fiber output by inserting an optical diffuser immediately before the pinhole. The diffuser scatters the light and makes the pinhole appear more like a point source. This allowed us to place various filters and a beam splitter (for intensity monitoring and feedback) between the fiber and the pinhole.

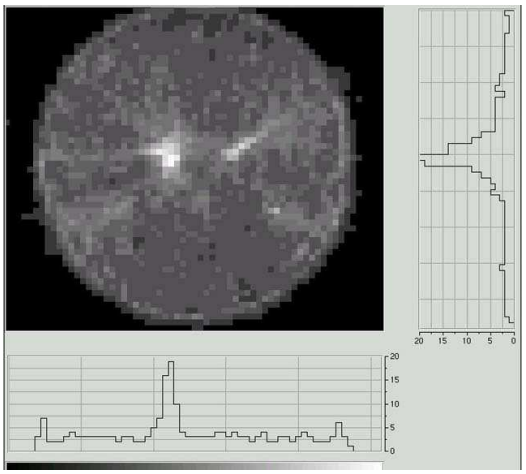

Figure 3.8: Image from the CCD of the spot when far out of focus and when the pinhole is as near as possible to the fiber output. Note: Focusing in and out significantly alters the intensity distribution, and at a location closer to focus the distribution approaches flatness. This image was made using a 10 micron pinhole.

Chapter 4

Software - MIRTS

Initially, the software we planned on using to control all of our experiments, was a soon to be highly modified version of Voodoo. Voodoo is an image capturing and utility package programmed in Java and developed by Scott Streit and Bob Leach for use with the electronics developed by Bob Leach of Astronomical Research Cameras, Inc.

After some deliberation and a fair amount of research, we decided that a new software package, developed in-house, would be the wisest choice. The reason behind this decision, was that in order to meet the requirements for our tests and to allow more control and customization of the experiment, we required absolute control over a software package that we understood.

I was the person chosen to undertake this task, and using Labview and C on a linux development platform, development on the Michigan InfraRed Testing Suite (or MIRTS) was begun.

4.1 Image Capturing - mirIC

The MIRTS package initially consisted of only the beginnings of a single program, known now as mirIC for Michigan InfraRed Image Capturing. The intended focus of this program was to initialize the Leach electronics by uploading the timing file, setting parameters, powering on the device, and allowing various types of image capturing. The lower case "mir" here only serves to indicate that the program is lower in the hierarchy than MIRTS. Its current status is a fairly well shaped image capturing program with the above capabilities as well as a stability that seems to at this point be better than Voodoo, although it is not yet as fully featured. The main human interface for mirIC shown in Figure 4.1 was designed to imitate Voodoo so that current users of Voodoo could easily migrate to it.

4.1.1 Development History

Due to a three month hiatus working at CERN, I was initially unable to contribute more than a non-working skeleton of the software program. Initial work on communicating with the Leach electronics was done in the summer of 2003 by another undergraduate, Joseph Paul. [9] By the end of the summer, Joe had made significant progress communicating with

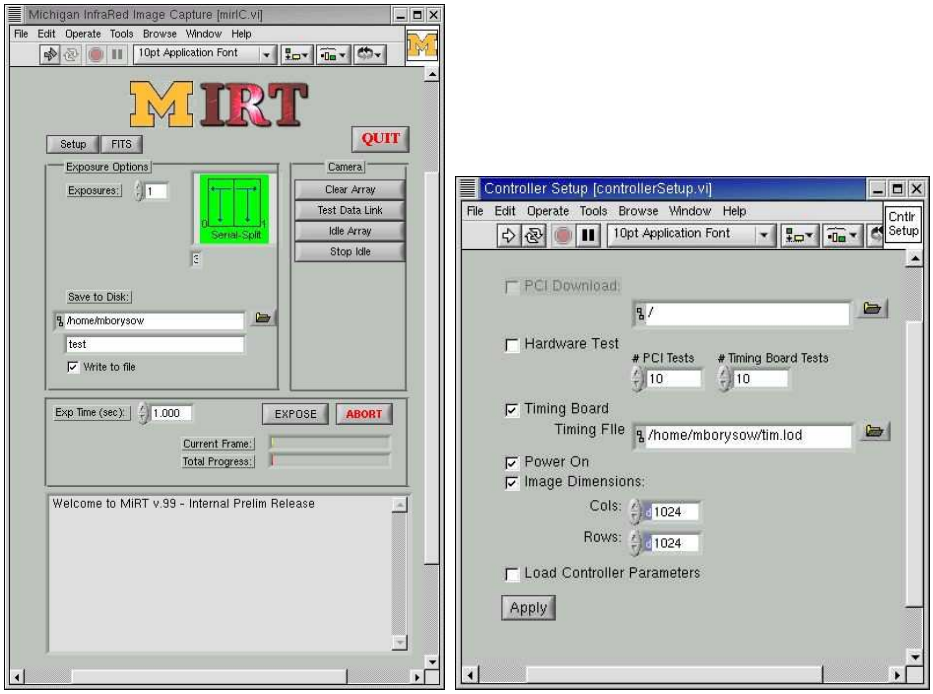

Figure 4.1: Screenshot of the main interface for the image capturing software mirIC (left) as well as a screenshot of its setup interface (right).

the electronics and was able to initialize the device. [10] He was able to acquire data from the device, but the images extracted were severely distorted. The package was, at the time, very unstable and was prone to crashes and lock ups of the PCI card that required rebooting the computer. But despite these problems, we were far ahead of where we had been three months prior.

When I returned to the group, control of the project was returned to me. I merged the skeletal structure I had developed at the beginning of the summer with the routines that Joe had made, and managed to fix most of the problems that caused crashes. After a large effort with the focus of making mirIC relatively modular and as crash-free as possible, the result was a quite stable, working program with which later motion control software could easily interact with. As of current, almost all the code has been entirely rewritten by myself. Only fragments of Joe's code and some pieces of Voodoo's DSP Routines in C remain.

4.1.2 Capabilities

Currently, mirIC allows timing board configuration, and a modular image capturing routine, that can be easily reconfigured to allow various types of image taking.

Under consideration is a programmatic modification to allow easier interaction with third party programs. This modification would amount to mirIC being toggled into "controlled mode," in which it would keep alert for a trigger in a configuration file. Once triggered, it would read all its parameters and options from a similar configuration file. This file would

be ASCII formatted so that it would easy to configure from various potential controlling third party software.

4.2 Motion Control - mirMC

Once the image capturing software was stabilized and usable, it was necessary to start programming a package to automate the stage motion and interact with the image capturing component. National Instruments provides a fairly full-featured library of tools, known as NI-Motion, from which one can construct virtually any kind of motion control package. Using this library, and a large number of intermediary analysis routines that I wrote in C, I was able to put together a package that satisfies our requirements for automation. The main interface of mirMC is shown in Figure 4.2.

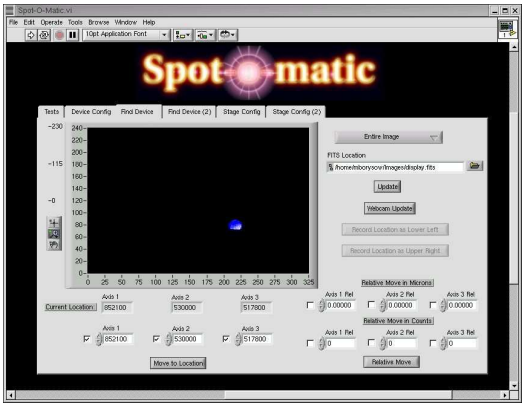

Figure 4.2: Screenshot of the main interface for the motion control software mirMC.

4.2.1 Capabilities

The software package mirMC is capable of doing the following:

- Focus on the CCD using one of two methods.
  - Intensity Squared Method
  - Finding the minimum measured spot size with a Knife Edge Test
- Define and follow the plane of the device by focusing at 3 points.
- Measure physical curvature of the CCD by focusing at many points on the device and calculate the deviations from a plane.

Partially or soon to be implemented:

- Referencing by pixel. I.e, can tell software to scan pixel at x=167 and y=10 and the software should find the pixel, focus in on it, and scan it.

Chapter 5

Webcam Characterizations

Now having a significant portion of the framework for our experiments in place, it became necessary to provide a more elaborate proof of concept. The plan was to run through the full spot-o-matic trials using a cheap CCD from a consumer class webcam.

5.1 Specifications

The device we would be testing was the CCD from a 3COM HomeConnect Webcam. The specifications of the device are as follows:

- 640x480 pixels, actual readout 320x240 due to linux driver limitations.
- 5um x 5um pixel dimensions.[1]
- Good quantum efficiency between 500nm and 1000nm (Silicon CCD).
- Easily interfaced for automation. (Has command line interface)

5.2 Measurements

The device was mounted in front of the spot-o-matic, as shown in Figure 3.2, and a series of scans were made. In the same figure, the end of the spot-o-matic can be seen, and looking closely at the webcam, one can see the razor blade which was used for the knife edge tests taped to the front.

[1] One result of our experimentation was finding out that each pixel response was actually a convolution of of a 3x1 array of pixels, oriented horizontally or vertically depending on region.

5.2.1 Intra-pixel Variations

A small region of the CCD was scanned using the 10 micron pinhole with the spot-o-matic focused on the CCD. The response of a pixel is recorded each time the stage is moved, and a map of pixel response vs. stage position is made. Some interesting features were observed while scanning several neighboring pixels.

The response map shown in Figure 5.1 is a convolution of the pixel response function and the relative spot intensity function. The analysis routines for deconvolving the two are not yet written, however it is a fairly simple procedure. One needs to go into frequency space by taking the fast fourier transform of the response map and dividing it by the fast fourier transform of the spot intensity function. Then perform the reverse transform and you should be able to recover the pixel response function.

Even without deconvolution, we have a small enough spot to resolve quite a bit of structure. It is clear from Figure 5.1 that we are actually reading out a 3x1 array of pixels, as opposed to a single pixel. Something like this was expected, since the CCD itself has 640 by 480 physical pixels and we are reading it out as a 320 by 240 pixel CCD. Looking at the size of the individual peaks, we can verify that the pixels are in fact roughly five micron square as quoted by 3COM. The 3x1 arrays seem to be oriented horizontally or vertically in regions.

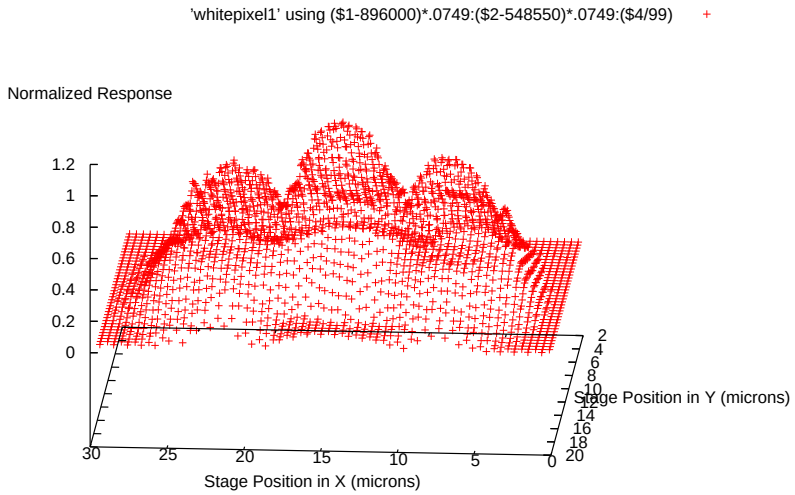

Figure 5.1: Intra-pixel variation of a single CCD pixel. Each data point is a representation of the value (intensity) reported by the pixel as a function of the stage coordinate x and y. In the readout mode we were using, it is clearly seen that effectively three pixels are being read out and some convolution of their responses is being reported. Also, if this is indeed the case, then there is evidence of gaps between the pixels where the device is not photon sensitive.

Interesting Discoveries

When looking at adjacent read out pixels, we see an interesting behavior. If you look at Figure 5.2 you will see that there is an overlap in the pixel response function. Two

neighboring read out pixels (neighbors in whichever direction the 3 pixels are oriented), share one of their 3 true pixels. In effect, each read out pixel only has one true pixel unique to itself, and two that are shared with its neighbors.

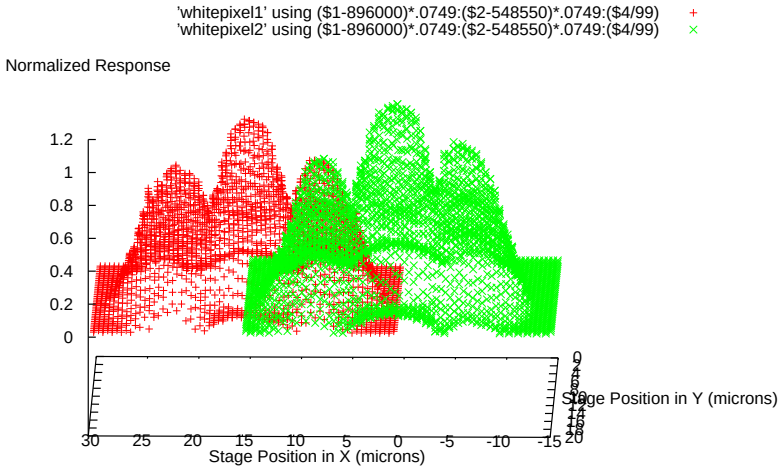

Figure 5.2: Intra-pixel variation of two adjacent CCD pixels shown in red and green. In the readout mode we are using, in addition to the response being some convolution of three pixel responses, we see that some pixels are shared.

Wavelength Dependence

Something worthy of keeping in mind is that we are working with a color CCD. In order for the CCD to report colors, we would expect some pattern of filters to be affixed or deposited very near to or directly on the CCD itself. In order to test this, similar scans will be conducted with narrow (10 nm FWHM) bandpass filters at 800 nm and 500 nm.

Chapter 6

Conclusions

The Michigan SNAP group has devised and constructed a facility in which we can perform high precision measurements on photosensitive devices.

I personally have developed all the software soon to be used to read out all devices tested in our lab using Generation II or III Leach Electronics, as well as all the software controlling the motorized stage which *intelligently* moves the spot-o-matic. I have also performed many tests to characterize both the stage and optics, and performed all of the analysis on that data in order to increase the precision of our final results. I have put in many hundreds of hours into this project and feel that I have contributed significantly in getting to the point where we are ready to test real devices with our newly assembled facility.

I feel that we can now claim with confidence, that we should be able to measure intra-pixel variation of the HgCdTe detectors to high precision within a short time frame.

Bibliography

[1] S.M. Carroll, "Why is the Universe Accelerating?," 2003, (see arXiv:astro-ph/0110414)

[2] S. Perlmutter, et al., "Measurements of Omega and Lambda from 42 High-redshift Supernovae," Ap.J. **517**, pp. 565-586

[3] A. Riess, et al., "Observational Evidence from Supernovae for an Accelerating Universe and a Cosmological Constant," A.J. **116**, pp. 1009-1038

[4] E.V. Linder, D. Huterer, "Importance of Suprernovae at $z > 1.5$ to Probe Dark Energy," 7 Aug 2002, (see arXiv:astro-ph/02080138v1)

[5] "Surpnova/Acceleration Probe - Fact Sheet," <http://snap.lbl.gov/pdf files/snapfacts.pdf>

[6] Snap Collaboration, "Supernova / Acceleration Probe (SNAP)," <http://snap.lbl.gov/pub/bscw.cgi/d92932/SNAP-SCI-00011.pdf>

[7] R.N. Hook, A.S. Fruchter, "Dithering, Sampling and Image Reconstruction," Astronomical Data Analysis Software and Systems IX, ASP Conference Proceedings **216** p. 521

[8] M. Wagner, Thesis at the Lawrence Berkeley National Laboratory, 2002

[9] Joseph Paul (2003), "Device Communication in Labview," August 2003 (unpublished).

[10] Joseph Paul (2003), "Summer 2003 REU Program," <http://www.physics.lsa.umich.edu/academics/research/Paul/japaul/>